Disentanglement of Orthogonal Hydrogen- and Halogen Bonds via Natural Orbital for Chemical Valence: a Charge Displacement Analysis

Gianluca Ciancaleoni,[a]* Leonardo Belpassi[b]

[a] Dipartimento di Chimica e Chimica Industriale, Università degli Studi di Pisa, via Giuseppe Moruzzi 13, Pisa 56124, Italy

[b] Istituto di Scienze e Tecnologie Chimiche "G. Natta"-CNR (CNR-SCITEC), c/o Dipartimento di Chimica, Biologia e Biotecnologie, Università degli Studi di Perugia, via Elce di Sotto 8, Perugia I-06123, Italy

*e-mail: gianluca.ciancaleoni@unipi.it

ABSTRACT

As known, the electron density of a covalently bound halogen atom is anisotropically distributed, with a region of low density on the elongation of the covalent bond (σ hole) and an accumulation orthogonal to the covalent bond. Therefore, halogen atoms are potentially able to establish many weak interactions, acting at the same time as a Lewis acid (halogen bond donor) and Lewis base (hydrogen bond acceptor). Indeed, there are many examples in which the halogen and hydrogen bond coexist in the same structure and, if a correct bond analysis is required, their separation is mandatory. We present here the advantage of coupling the Charge Displacement analysis with Natural Orbital for Chemical Valence method to separately analyze orthogonal weak interactions, for both symmetric and asymmetric adducts. The methodology gives optimal results with intermolecular adducts but, in the presence of an organometallic complex, also intramolecular interactions can be correctly analyzed. Beyond the methodological aspects, it is shown that correctly separate and quantify the interactions can give interesting chemical insights about the systems.

INTRODUCTION

The halogen bonding (XB),[1,2] i.e. the inter- or intramolecular interaction that exists between a Lewis base and a polarized halogen, has many peculiarities that in the last years have been investigated. For

example, it is highly directional,[3,4] as the σ hole (the region with a positive electrostatic potential) is always located at 180° of the covalent bond; further, the low degree of hybridization typical of heavier halogen atoms, which are the most prone to XB, makes the lone pairs to be almost purely *p* in character and, consequently, at 90° of the covalent bond. This means that the halogen atom can act at the same time as a Lewis acid (LA), using its σ* orbital to accept electronic density (XB donor) and as a Lewis base (LB), by using its lone pairs to establish, for example, a hydrogen bond (HB acceptor).

Indeed, there are many examples of molecular systems in which the two interactions coexist.[5–11] When it happens, it would be desirable to characterize them separately, in order to provide a correct bond analysis for each of them, but this can be not straightforward. Especially when the charge transfer is very small,[12–14] the localization-based methods are less reliable, whereas a density-based ones (as Charge Displacement, CD), would still give reliable results. In the past, CD-computed charge transfers have been fruitfully coupled with various experimental techniques, demonstrating good correlations and giving an elegant theoretical framework to rationalize experimental results.[12,15–18]

And indeed, the CD function analysis[19] demonstrated to be a greatly useful bond analysis tool in the characterization of a wide range of chemical interactions, from the coordinative bond[18,20,21] to noncovalent ones.[12,15,22–24] The CD methodology was initially based on the integration of the electron density difference ($\Delta\rho$) between the adduct and the isolated fragments. For symmetric systems, $\Delta\rho$ could be separated into contributions on the basis of the irreducible representations of the point group to which the system belongs.[18,25,26] These contributions demonstrated to be ideal to describe the Dewar-Chatt-Duncanson (DCD) contributions[27,28] of the coordinative metal-ligand bond.

Successively, the CD analysis were coupled with the Natural Orbital for Chemical Valence NOCV) theory[29–32], defining the NOCV-CD approach.[33] In the NOCV method, the electron density difference ($\Delta\rho$') is not defined respect to the wavefunctions of the isolated fragments, but respect to their antisymmetrized product ("promolecule"). For single-determinant wavefunctions, $\Delta\rho$' can be brought into diagonal contributions using the "valence operator" $\hat{V}$, producing pairs of orbitals with the same *eigenvalue* (in absolute value) that describes the donor and acceptor molecular orbitals involved in the charge rearrangement.[33] When applied to organometallic complexes, also the NOCV demonstrated to correctly decompose donation and back donation for asymmetric systems.[34–37] The method can be also applied in combination with the Extended Transition State – Natural Orbital for the Chemical Valence (ETS-NOCV),[38] so that an energy stabilization can be associated with the different bonding components. We point out that both the NOCV-CD and ETS-NOCV are based on the assumption that the molecular system can be separated into chemically meaningful reference fragments

and clearly this assumption is not always valid or unambiguous. For completeness, we have to remind that the partitioning of different bonding components one may obtain both in the framework of NOCV-CD and ETS-NOCV are solely related with the inter-fragments orbital relaxation term, which may be not even the dominant contribution to the interaction (others energetic terms are the Pauli repulsion and electrostatic interaction).

Regarding the XB, in many cases a decomposition into contributions has been generally not necessary, because in the reported cases the total $\Delta\rho$ was already a good descriptor of the interaction under study.[12,39] But, recently, the NOCV method demonstrated to be a useful tool in the analysis of bifurcated halogen[40] and chalcogen bonding[41], and in recent cases in which XB and HB co-exist, regarding urea[42] and selenourea,[43] the NOCV revealed that the two weak interactions could be separated.

Inspired by these papers, we decided to use the CD analysis in the characterization of selected examples of adducts with co-existing XB and HB, taking advantage of the NOCV procedure and taking into account different adducts of increasing difficulty (Scheme 1). The NOCV analysis already gives an estimation of the energy contribution of each channel and there are already tools to estimate the charge flux corresponding to each component (as NBO,[44] or Mulliken and Hirshfeld population analyses implemented in ADF2017[45]), but there are some advantages in using the CD analyses that cannot be ignored: for example, it does not give just a number but provides valuable information on the flux throughout the whole adduct, allowing its quantitative measurement. This property allowed to correctly assess the interplay between back-donation and polarization in determining the IR stretching frequency of organometallic carbonyls.[18] Last but not least, the CD tool can be used also in conjunction with the freely available software ORCA,[46,47] which recently added the computation of NOCV pairs among its many functionalities,[48] benefiting a potentially wider community.

Here, we start with a C_{2v}-symmetric molecular adduct, in order to apply both the methods, that based on irreducible representation and the NOCV-CD one, made by a bi-substituted pyridine having aniline moieties (**PyS**). The nitrogen of the pyridine is good a XB acceptor, while the amino protons of the aniline are HB donors. Then, we pass to asymmetric adducts using selenourea (**SeU**) and I_2 or N-X-succinimides, with X = Cl, Br and I (NXS). Using NXS, we have three interactions at the same time as, in addition to the XB and HB on the halogen atom, the amino proton of **SeU** can interact also with the oxygen. Finally, a Rh(I) organometallic complex, **RhP2**, a simplified version of a complex recently synthesized,[49] is studied, where the XB is intramolecular and the fragmentation is not as obvious as in the previous cases.

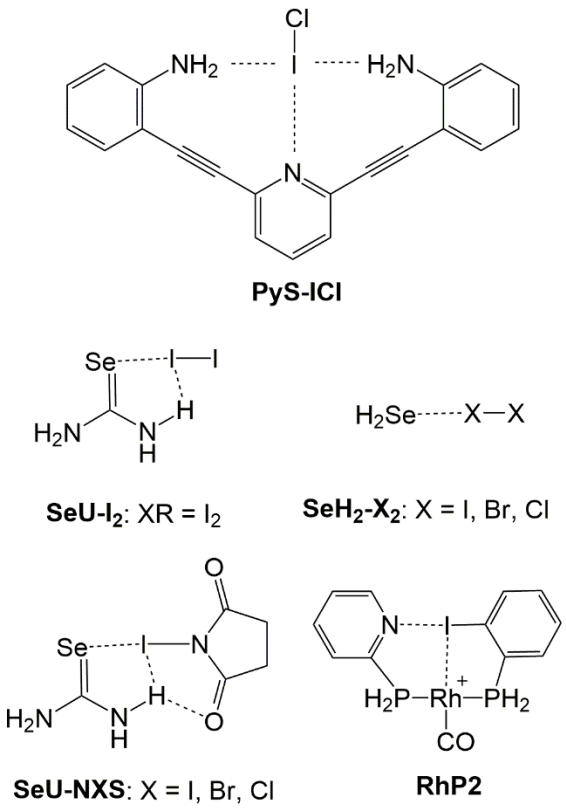

Scheme 1. Abbreviations and structure of the adducts studied.

Beyond the methodological aspects, it will be shown that correctly quantify the interactions can give interesting chemical insights about the systems under study.

RESULTS AND DISCUSSION

Symmetric XB-bonded adducts are not common. Here, we decided to use a model system, not unrealistic[50] but yet to be investigated, a pyridine substituted in 2,6 positions with 1-amino-2-ethynyl-phenyl groups (**PyS**). This leads to a planar molecule belonging to the C_{2v} point group, having four irreducible representations, A_1, A_2, B_1 and B_2. In this molecular framework, a R-I moiety can interact at the same time with the nitrogen and the amino groups, establishing both a XB between the lone pair of the pyridine and the σ hole of the iodine and a HB between the amino groups and the lone pairs of the iodine. In order to effectively make use of the symmetry, the iodine has been imposed to be exactly between the two amino protons and the geometry adduct has been partially optimized using the symmetry constrain. This leads to a system that is not exactly the energy minimum, the energy

difference is 7.5 kcal/mol, but, importantly, it still preserves all the chemical features of a realistic system and still belongs to the C_{2v} point group.

It is interesting to note that in the fully relaxed geometry, the iodine tends to establish a covalent bond with the nitrogen (N···I distance 2.405 Å) and weakened bond with the chloride (I···Cl distance 2.521 Å, bond distance for isolated ICl 2.391 Å), in a typical substitution pattern[41] and forming an incipient ion pair (**PySI**)$^{+}$Cl^{-}. This is not uncommon when a pyridine is involved in a XB adduct.[51]

For this system, the EDA as implemented in ORCA 4.1, shows a ΔE_{int} = -21.7 kcal/mol, which can be decomposed in ΔE_{oi} = -17.7, ΔE_{st} = 5.5 and ΔE_{disp} = -9.5 kcal/mol. It can be noted that the orbital contribution is quite large. By using ADF2014, it is also possible to decompose the Pauli (ΔE_{Pauli}) and electrostatic (ΔE_{elst}) contributions, the sum of which is ΔE_{st}. They result to be ΔE_{Pauli} = 28.9 and ΔE_{elst} = -21.9 kcal/mol (ΔE_{st} = 7.0 kcal/mol), confirming that also the electrostatic contribution is not negligible (Table S1 and S2, Supporting Information).

By using the second order perturbation theory analysis of the Fock matrix, as implemented in NBO, there is a donation from the lone pair of the nitrogen to the σ*(I-Cl) with a $E^{(2)}$ = 13.9 kcal/mol and two donations from the lone pair of the iodine to the two σ*(H-N), each with a $E^{(2)}$ = 5.7 kcal/mol. Therefore, the presence of two interactions orthogonal in space, XB and HB, is confirmed.

Given the symmetry of the adduct, it is possible to decompose the electron density difference $\Delta\rho$ in four contributions from different irreducible representations. As shown in Figure 1, the A_1 component comprises depletion regions on the pyridine moiety, an accumulation region between the nitrogen and iodine and accumulation regions on the ICl fragment, all of them with an axial symmetry with respect to the N···I (*z*) axis. Such pattern describes the XB between the nitrogen and the iodine and the consequent polarization of the aromatic ring and the I-Cl bond due to the charge transfer and electrostatics. Very small depletion regions are present on the amino groups, but far from the N···I isoboundary (see later), therefore they are expected to not influence the results very much.

The B_2 component shows polarization regions on the nitrogen (accumulation) and the chlorine (depletion), and a series of accumulation/depletion regions on the *y* axis, involving the amino groups and the iodine. These regions are compatible with the HB between the lone pairs of the iodine and the hydrogen atoms. In particular, the small depletion region present on the hydrogen directly pointing toward the iodine is peculiar of HBs.[12] The depletion region on the chlorine can be interpreted as a weakening of the π structure of the ICl bond by the formation of the HB.

A_2 and B_1 components (see Supporting Information) only contains polarization contributions not related to the weak interactions discussed here.

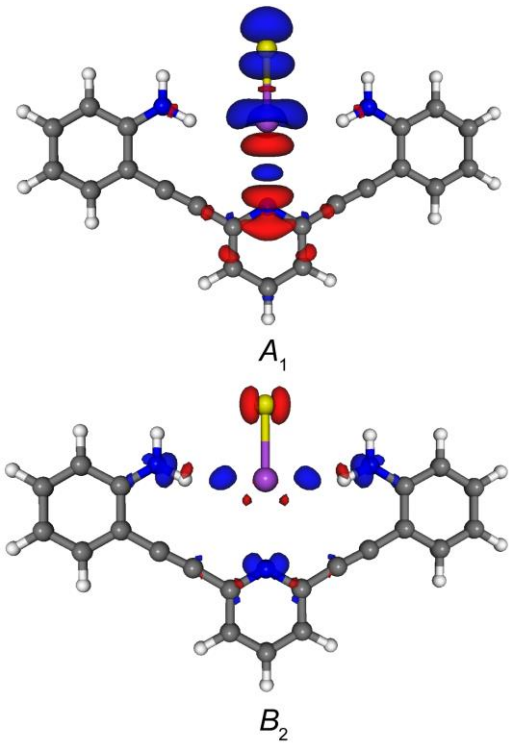

Figure 1. Isodensity surfaces (1 me a.u.$^{-3}$) for the deformation maps relative to two irreducible representations of $\Delta\rho$ of the [**PyS**]$^{\cdots}$[ICl] adduct. The charge flux is red → blue.

Now the contributions can be separately integrated to obtain the corresponding CD functions and separately quantify the weak interactions. From the methodological point of view, two problems arise. The first problem is related to the integrating axis, that cannot be the same for the two interactions. If we define *z* the axis passing for the nitrogen and the iodine, we can effectively integrate the A_1 contribution and quantify the XB, but *z* is orthogonal to the HB direction and no information can be derived about the HB. Therefore, $\Delta\rho_{B2}$ must be integrated along *y*.

The second problem is about the definition of the interatomic boundary. According to the CD methodology, the boundary between the two fragments is typically defined as the point on the integrating axis at which equal-valued isodensity surfaces of the isolated fragments are tangent. Despite this definition is clearly arbitrary, it works very well with linear adducts and not too complicated organometallic complexes, but it is inapplicable in this case, as the two fragments are interpenetrated. For a system like this, we are aware that any attempt to find a suitable boundary between the two fragments is questionable. Anyway, a simple possibility is to build another adduct similar to that under study but simpler, calculate the boundary and translate the information. In this case, the complex

between an unsubstituted pyridine and ICl, with the same N···I and I···Cl interatomic distances, is a good reference for the XB, while the adduct between ICl and aniline, again with the same H···I and I···Cl relative positions, can be used for the HB. Not only, but even if providing a single number is useful for the quantification of the interactions and their comparison, the most important thing is the analysis of the whole CD curve, especially in the region between the interacting fragments.

Having in mind these issues, the integration of $\Delta\rho_{A1}$ along z leads to the function CD_{A1} shown in Figure 2. The curve is always positive, indication that the electronic flux and polarization are always from right (nitrogen) to left (iodine). At the boundary, the value of the curve (CT_{A1}) is 0.115 e. Such value lies in a region in which Δq varies very smoothly with z, therefore a small "error" on the boundary position does not affect the value very much.

On the other hand, integrating $\Delta\rho_{B2}$ along y leads to CD_{B2}. Here the curve is more complicated, but fully understandable looking at the corresponding deformation map (Figure 2). In the negative semiaxis of y the curve is positive, as the electronic flux is from right (iodine) to left (proton). At positive values of y, the curve is negative, as here the electronic flux is from left (iodine) to right (proton). The shape and numerical values of the two sections are dictated by the co-presence of the HB and the polarization regions on the nitrogen and the chlorine. As a net result, CT_{B2} is 0.003 e. In this case, the boundary lies on a minimum, therefore any small movement of the boundary produces a large (in percentage) variation of CT_{B2}. Anyway, in absolute value the difference is not that much, as we can say that CT_{B2} can vary between 0.003 and 0.014 e, depending on the method chosen to evaluate the boundary position.

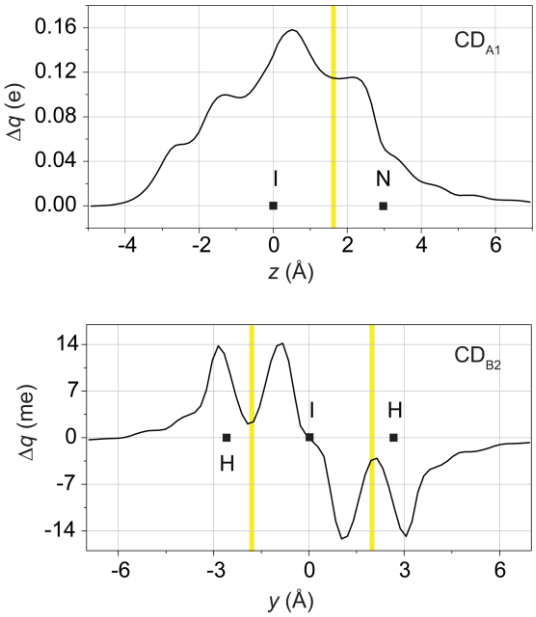

Figure 2. Symmetry-separated Charge Displacement functions (CD_{A1} and CD_{B2}) curves for the [**PyS**]···[ICl] bond. Black dots indicate the position on the axis of the atomic nuclei. A yellow vertical band indicates the boundary between the fragments.

Applying the NOCV analysis on the same adduct, only the first two orbital pairs are relevant, having an orbital energy content of -10.8 and -3.4 kcal/mol for k = 0 and 1, respectively. All the other components contribute for less than 0.7 kcal/mol each. Visualizing the electron density difference maps $\Delta\rho'_0$ and $\Delta\rho'_1$ (Figure 3), it appears evident that $\Delta\rho'_0$ is strikingly similar to $\Delta\rho_{A1}$, both of them describing only the N···I XB and the consequent fragments polarization. Interestingly, in $\Delta\rho'_0$ no accumulation/depletion regions are present on the amino groups. On the other hand, $\Delta\rho'_1$ is similar to $\Delta\rho_{B2}$ but it does not contain the polarization regions on the nitrogen and the chlorine, as $\Delta\rho_{B2}$ does. Indeed, such polarization contributions can be found in other NOCV pairs, for example that with k = 4, associated to negligible energy content (-0.35 kcal/mol).

Therefore, not only the NOCV methodology is as good as the symmetry-based analysis in describing the weak interactions, as already known for systems with similar symmetry,[42] but in some cases, it can also be better, with a more efficient separation of the chemically relevant contributions. Also the integrated CD functions are qualitatively similar, with only small numerical differences. At the isoboundary CT_0 is 0.128 e, which are not far from the values derived through the symmetry separation. Regarding CT_1, it is 0.015 e, which is quite different from CT_{B2}, but in this case the HB is

better separated from the polarization contributions and the slope around the boundary is smaller, then the NOCV value is more reliable than the estimation from the symmetry-separation methodology.

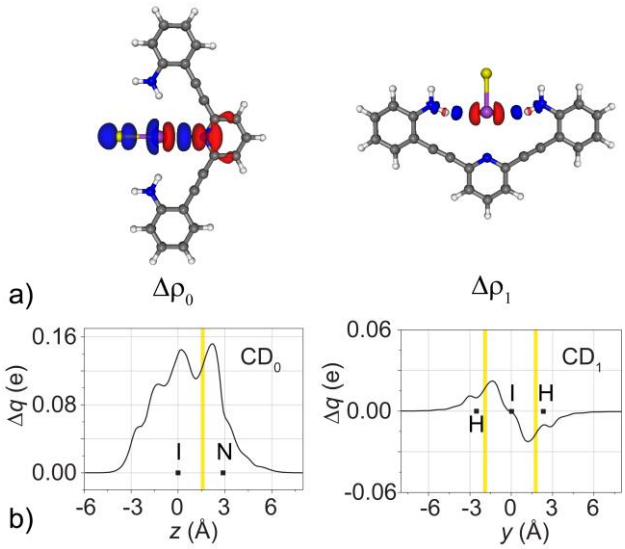

Figure 3. a) Isodensity surfaces (2 me a.u.$^{-3}$) for the deformation maps relative to the $\Delta\rho_k$ (k = 0-1) contributions of the [**PyS**]···[ICl] adduct (the charge flux is red → blue); b) charge displacement functions (CD_0 and CD_1) curve for the [**PyS**]···[ICl] bond. Black dots indicate the position on the axis of the atomic nuclei. A yellow vertical band indicates the boundary between the fragments.

Therefore, it is possible to decompose the two orthogonal interactions by using both the methodologies with similar results. This conclusion is particularly important because C_{2v} symmetric adducts having both XB and HB are not so common, therefore the NOCV-CD analysis appears very interesting to reliably study real cases.

The first real case will be about the adducts between **SeU** and various XB. For the fully relaxed adduct between **SeU** and I_2, the EDA gives ΔE_{int} = -22.7 kcal/mol, ΔE_{oi} = -36.3, ΔE_{st} = 18.1 and ΔE_{disp} = -4.5 kcal/mol (see Supporting Information for the decomposition of ΔE_{st}). According to NBO analysis, the donation lp(Se) → σ*(I-I) is associated with an energy of 63.4 kcal/mol, whereas the lp(I) → σ*(H-N) one is associated to an energy of 5.6 kcal/mol. Again, the orbital contribution is relevant and there are two weak interactions at the same time.

The NOCV analysis gives two important contributions of -29.8 ($\Delta\rho'_0$) and -3.4 kcal/mol ($\Delta\rho'_1$), of which the corresponding three-dimensional electron density deformation maps are visible in the Supporting Information.

It is evident that the XB and HB still have a different local symmetry, but in this case the separation is not perfect and, lowering the threshold to 0.8 me a.u.$^{-3}$, $\Delta\rho'_1$ shows a small accumulation region also between the selenium and the iodine. The small involvement of the selenium in the HB can be due to the fact that the two interactions are not perfectly orthogonal as the angle Se-I-H is 61.5°, but the introduced error seems negligible in this case. The quantification of the interactions leads to a CT_0 of 0.323 e, relative to the XB, and a CT_1 of 0.030 e, relative to the HB. In this case the integration axes are Se···I (z) for $\Delta\rho'_0$ and H···I (y') for $\Delta\rho'_1$ and not simply y.

Increasing again the complexity of the system, it is possible also to have three weak interactions at the same time. For example, in **SeU-NBS**, beyond the Se-Br XB, the hydrogen of the amino group is potentially able to interact with both the iodine and the oxygen of the succinimide moiety. Also in this case, a symmetrization of the system to separate the contributions is not possible, but the NOCV analysis can be performed the same. The results are shown in Figure 4: the first contribution (ΔE_0 = -10.8 kcal/mol) is again corresponding to the Se···Br XB, with the usual depletion/accumulation regions pattern and a CT_0 of 0.333 e. The second contribution (ΔE_1 = -3.4 kcal/mol) mainly corresponds to the H···Br HB, associated with a CT_1 of 0.021 e. Anyway, a careful inspection of $\Delta\rho'_1$ shows that a small depletion region exists on the oxygen of the NBS, likely due to polarization effects. This small negative region interferes with the quantification of the Br → H electronic flux, as CT_1 is the sum of the two contributions. As a result, the charge transfer involved in the H···Br HB is slightly underestimated by CT_1. $\Delta\rho'_2$ describes a polarization of the selenourea, with a charge flux from the nitrogen atoms to the selenium, as already observed for other XB selenourea-adducts[52] and complexes.[34,43] Finally, $\Delta\rho'_3$ (-1.7 kcal/mol) describes the H···O HB, depletion regions on the oxygen with a shape resembling a p orbital and accumulation regions between the two atoms and on the nitrogen. This contribution is particularly weak, but it is expected that a HB of this kind is mainly electrostatic in nature and contains only a small orbital contribution,[53] which is the only analyzed here. Further, other accumulation/depletion regions are present on the selenium and iodine. As the region on the iodine is located exactly on the boundary between hydrogen and oxygen, the quantification of this contribution cannot give information about the HB, as CT_3 is the sum of two regions of comparable intensity.

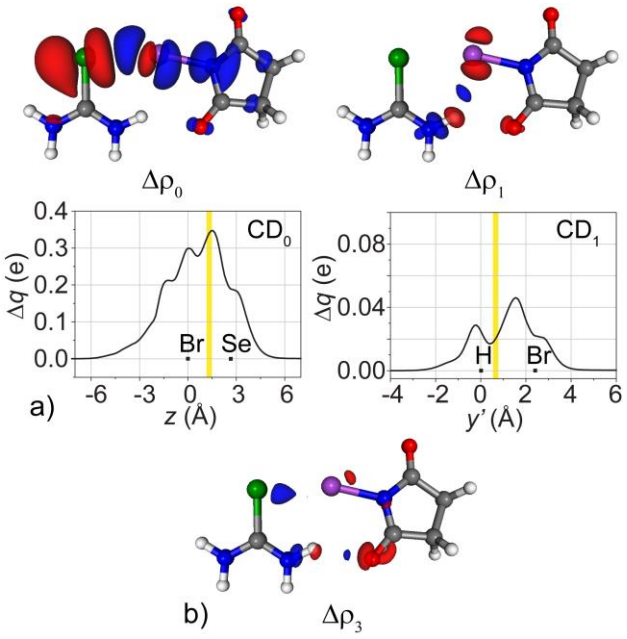

Figure 4. a) Isodensity surfaces (2 me a.u.$^{-3}$) for the deformation maps relative to the $\Delta\rho'_0$ and $\Delta\rho'_1$ contribution of the [**SeU**]···[NBS] adduct (the charge flux is red → blue) and charge displacement functions (CD_0 and CD_1) curve for the [**SeU**]···[NBS] bond. Black dots indicate the position on the axis of the atomic nuclei. A yellow vertical band indicates the boundary between the fragments; b) Isodensity surfaces (1.4 me a.u.$^{-3}$) for the deformation maps relative to the $\Delta\rho'_3$ of the [**SeU**]···[NBS] adduct.

From the analysis of the homologues NCS and NIS, something unexpected emerges. The total interaction energy, with respect to relaxed fragments (ΔE_{tot}), is -26.2, -27.3 and -15.8 for [**SeU**]···[NIS], [**SeU**]···[NBS] and [**SeU**]···[NCS], respectively, whereas one of the pillar of halogen bonding is that heavier halogens give stronger XBs, with numerous experimental and theoretical confirmations[2] and only one counter-example.[54] Obviously, ΔE_{int} depends on all the interactions, therefore in this case the disentanglement of XB results to be particularly interesting. Moreover, ΔE_{int} takes into account also the electrostatic interaction between the fragments, which always plays an important role in HBs and XBs.[55] Interestingly, the trend of the dissociation energies is slightly different: -20.3, -18.3 and -11.6 kcal/mol for NIS, NBS and NCS, respectively. The difference lies in the preparation energy of NBS (6.8 kcal/mol), which is larger than that of NIS (4.7 kcal/mol).

According to the CD results, the framework for all the [SeU]···[NXS] adducts remains exactly as described for [**SeU**]···[NBS], but obviously there are differences from the quantitative point of view. It appears evident that substituting the bromine with iodine or chlorine, the strength and the amount of

charge transferred diminish (ΔE_0 and CT_0 are -10.6 kcal/mol and 0.307 e for **SeU-NIS** and -18.1 kcal/mol and 0.200 e for **SeU-NCS**, see Table 1). Again, this is an unexpected trend.

Table 1. NOCV-separated charge-transfer values (CT_k, in e), orbital energy for the adduct formation (ΔE_{oi}, in kcal/mol) and orbital energies associated with the *k*-th NOCV pair (ΔE_k, in kcal/mol).

Fragments	CT_0 [a]	CT_1 [b]	ΔE_{oi}	ΔE_0	ΔE_1
PyS···ICl	0.128	0.015	-17.7	-10.8	-3.4
SeU···I$_2$	0.323	0.030	-36.3	-29.8	-3.4
SeU···NIS	0.307	0.019	-41.3	-32.1	-4.3
SeU···NBS	0.333	0.021	-45.3	-35.9	-3.6
SeU···NCS	0.200	0.021	-23.2	-18.1	-2.3
SeH$_2$···NIS	0.115 [c]		-12.2	-10.6	-0.4
SeH$_2$···NBS	0.090 [c]		-9.2	-8.2	-0.2
SeH$_2$···NCS	0.043 [c]		-4.0	-3.6	-0.1

[a] Integrated along the N-halogen (or Se-Halogen) axis; [b] integrated along the H-Halogen axis; [c] CT_{tot}

And, indeed, considering a simple series of XB adducts in which the HB is not present, as SeH$_2$-NXS (see Supporting Information), the trend is the expected one: ΔE_{int} is -8.4, -6.3 and -4.0 kcal/mol for X = I, Br and Cl, respectively, whereas the corresponding values of CT_{tot} are 0.115, 0.090 and 0.043 e. The difference between the two trends can be explained considering the adduct geometries.

In the SeH$_2$-NXS series, the Se···X distance depends only on the strength of the XB and is 3.177, 3.109 and 3.243 Å for I, Br and Cl, respectively. Normalizing these values to the sum of the van der Waals radii, they are 0.82, 0.83 and 0.89, respectively. Coherently, when only XB is important, the normalized bond distance increases going from iodine to chlorine.

For the **SeU**-NXS series, the Se···X distances are 2.910, 2.737 and 2.867 Å for iodine, bromine and chlorine, respectively. The normalized distances are 0.75, 0.73 and 0.78. In this peculiar case, the normalized distance is smaller for the bromine, likely because of the presence of the HB that influences the geometry of the adduct and, consequently, the strength of the XB. In this particular case, the correct separation and quantification of the two weak interactions has been important to have an additional insight in the chemistry of the adduct and explain the anomalous trend.

Finally, as a last example, we can focus on a recently synthesized organometallic complex, in which the iodophenyl moiety interacts intramolecularly with a pyridine of a different ligand by XB and with

the rhodium(I) by an intramolecular HB. Here the situation is particularly complicated because, being intramolecular interactions, also the fragmentation is an issue. It is evident that the fragmentation would be generally difficult for an organic adduct, but not impossible of course,[42] having intramolecular XB. But given the structure of the complex and since the NOCV-CD methodology have been successfully used to characterize metal-ligand bonds, there are two possible fragmentation: $[Rh(CO)(P^1H_2Py)]^{+\cdots}(P^2H_2PhI)$ and $[Rh(CO)(P^2H_2PhI)]^{+\cdots}(P^1H_2Py)$.

Anyway, only the latter is interesting as in the former (see Supporting Information) both XB and Rh-I interactions are entangled and mixed with other contributions coming from the P^2-Rh bond.

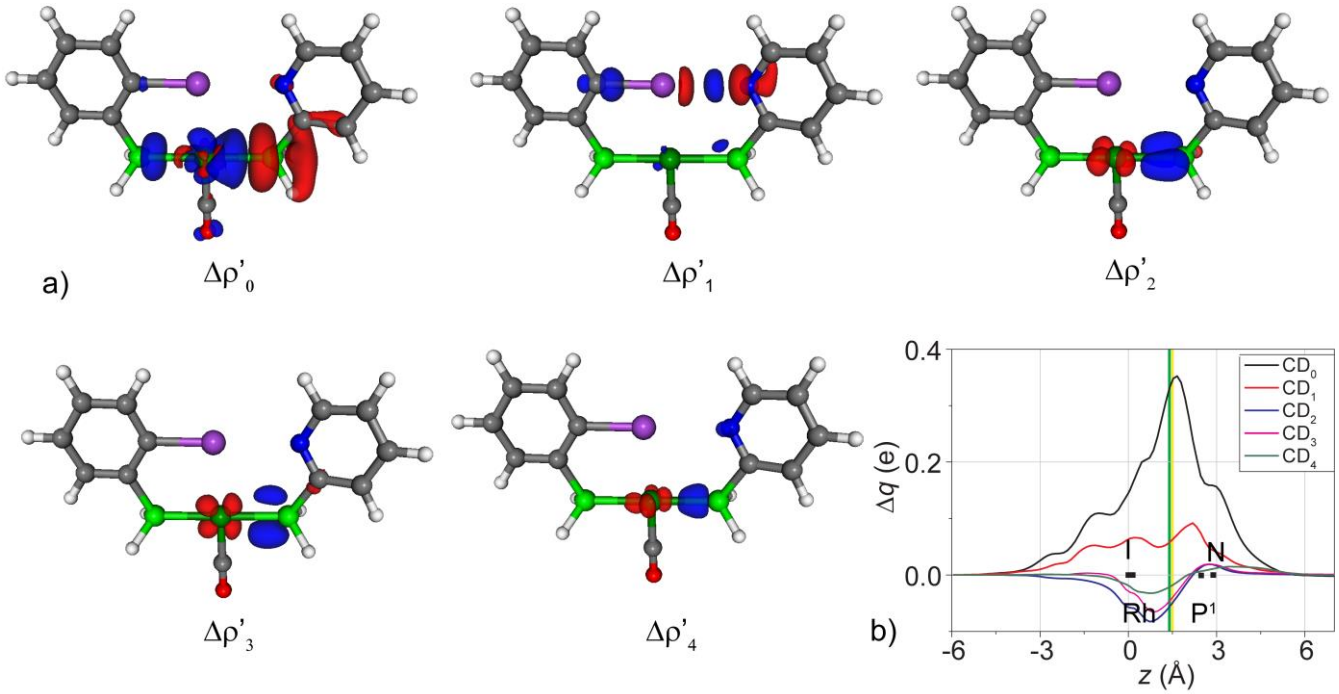

Figure 5. a) Isodensity surfaces (2 me a.u.$^{-3}$) for the deformation maps relative to the $\Delta\rho'_k$ (k = 0-4) contributions of the $[Rh(CO)(P^2H_2PhI)]^{+\cdots}(P^1H_2Py)$ adduct (the charge flux is red → blue); b) charge displacement functions (CD_k, k = 0-4) curves for the $[Rh(CO)(P^2H_2PhI)]^{+\cdots}(P^1H_2Py)$ bond. Black dots indicate the position on the axis of the atomic nuclei. A green (yellow) vertical band indicates the $Rh^{\cdots}P^1$ ($N^{\cdots}I$) boundary between the fragments.

Therefore, considering the $[Rh(CO)(P^2H_2PhI)]^{+\cdots}(P^1H_2Py)$, the NOCV analysis leads to the presence of five important contributions (ΔE_{oi} = -63.7, ΔE_0 = -35.1, ΔE_1 = -7.7, ΔE_2 = -6.7, ΔE_3 = -5.9, ΔE_4 = -3.5 and ΔE_5 = -1.1 kcal/mol), each of one associated with a different $[Rh(CO)(P^2H_2PhI)]^{+\cdots}(P^1H_2Py)$ bond component. Indeed, as Figure 5 shows, $\Delta\rho'_0$ is associated with the P^1 → Rh σ donation, $\Delta\rho'_1$ with the N

→ I XB (with a very small perturbation on the P^1-Rh bond that likely introduces a small numeric error on the quantification of the XB), $\Delta\rho'_2$ and $\Delta\rho'_3$ are associated with the P^1 ← Rh π back-donation and, finally, $\Delta\rho'_4$ is associated with a small P^1 ← Rh σ back-donation. Noteworthy, in this case the two important axes, N-I and Rh-P^1, are parallel and therefore the use of one of them (here, the N···I axis) is enough to extract all the information. The Rh···P^1 and N···I isoboundaries are slightly different and can be computed again by using model systems ($[Rh(CO)_2(PH_3)]^+$···(PH_3) and Py···IC_6H_5, respectively). It has to be also noted that the *eigenvalues* associated to k = 1 ad 2 are quite similar (0.273 and 0.256, respectively), but the local symmetry of the two interactions are very different, one of which showing a σ symmetry and the other having a π symmetry with respect to the chosen axis (see Figure 5). Hence, each function can be separately integrated, obtaining a quantification for all the contributions: the σ donation accounts for 0.348 e, the XB for 0.065 e, the two π back-donation contributions can be quantified in -0.045 and -0.037 e and the σ back-donation accounts for -0.015 e.

The Rh-I interaction is not visible in this fragmentation because it exists already in the initial fragment and therefore it never appears in the difference maps between the adduct and the fragments. No other reasonable fragmentation scheme is possible, then the NOCV method cannot give information about that interaction. Anyway, according to us, the quantitative characterization of the orbital terms for the XB and the Rh-P^1 bond at the same time is already a good result considering the complexity of the system. Clearly, we are not able to separate the electrostatic and Pauli terms of the two interactions, as in previous cases, but in many contexts the estimation of the orbital term would be enough.

More in general, we can add that the NOCV-CD methodology always give some information, but whether the latter are complete and chemically unambiguous may depend on the specific complexity of the system. Thus, higher completeness and accuracy can be obtained when the adduct is "simple" (only one interaction is present or two, but with different local symmetry), but when the system presents a more complex pattern of interactions, its accuracy and/or completeness can be affected.

CONCLUSIONS

In conclusion, we reported the results of a study on the bond analysis of adducts held together by numerous weak interactions. In all the cases, the CD methodology is able to characterize the different contributions and give quantitative information, taking advantage of the NOCV analysis for their disentanglement. The NOCV methodology proved in some cases to decompose the different components even better than the symmetry-based method. The important thing is that the local symmetries of the interactions are different, as generally the XB and the HB are. Their orthogonality,

indeed, facilitates the separation. From the chemical point of view, we showed that having multiple weak interactions can also lead to unexpected results, as in the case of the selenourea and N-halogen succinimide, in which the bromine-based XB resulted stronger than the corresponding iodine-based one, both in terms of interaction energy and charge displaced. This anomalous result is due to the fact that the Se···X distance is not dictated exclusively by the XB strength, as generally is, but also to the strength of the HB, which leads to a normalized Se···Br distance smaller than the Se···I one. In a general sense, this case is particularly instructive, because even if it has been easy to rationalize, it was not easy to predict, as the presence of many interactions can lead to unexpected results.

Also in the most complicated cases, as in the organometallic Rh(I) system we considered here, the XB can be efficiently separated by the different DCD components of the P-Rh bond, with a separate estimation of all of them by CD analysis. This example underlined the importance of the adopted fragmentation scheme and pointed out that some interactions could be so entangled with others to be impossible to separate. In those cases, a further simplification of the system could be done or other tools should be used.

COMPUTATIONAL DETAILS

If not otherwise specified, all the geometries were optimized with ORCA 4.1.0,[46,47] using the B3LYP functional and the RIJCOSX approximation in conjunction with a triple-ζ quality basis set (OLD-ZORA-TZVP for iodine and rhodium, ZORA-TZVP for all the others, grid = 4). Relativistic effects were treated with the scalar zeroth-order regular approximation (ZORA).[56] B3LYP proved to be quite reliable for XB adducts.[57] All the structures were confirmed to be local energy minima (no imaginary frequencies). Dispersion effects were accounted using the Grimme D3-parametrized correction with Becke–Jonhson damping to the DFT energy.[58]

For symmetric systems, the optimization was carried out using ADF package (v.2014) using the B3LYP functional. A triple zeta basis set with two polarization functions was used on all atoms (TZ2P, except for iodine, for which the QZ4P basis set was used) with a small frozen core. Relativistic effects where included by means of ZORA Hamiltonian.

Energy decomposition analysis.[59] The EDA has been performed using the same computational details used for geometry optimization. The EDA allows the decomposition of the bond energy into physically meaningful contributions. The interaction energy (ΔE_{int}) is the difference of energy between the adduct and the unrelaxed fragments. It can be divided into contributions associated with the orbital, steric and dispersion interactions, as shown in eqn (1)

$$\Delta E_{int} = \Delta E_{st} + \Delta E_{oi} + \Delta E_{disp} \quad (1)$$

For the total interaction energy (ΔE_{tot}), also the preparation energy has been calculated (eqn 2)

$$\Delta E_{tot} = \Delta E_{int} + \Delta E_{prep} \quad (2)$$

ΔE_{st} is usually called the steric interaction energy and it is the sum of ΔE_{elst}, the classical electrostatic interaction between the unperturbed charge distributions of the fragments (ρ_A and ρ_B) at their final positions in the adduct, and the Pauli repulsion (ΔE_{Pauli}) that is the energy change associated with going from $\rho_A + \rho_B$ to the antisymmetrized and renormalized wave function. The decomposition of ΔE_{st} is not possible with ORCA 4.1.0. ΔE_{st} comprises the destabilizing interactions between the occupied orbitals and is responsible for any steric repulsion. ΔE_{oi} is the contribution arising from allowing the wave function to relax to the fully converged one, accounting for electron pair bonding, charge transfer and polarization, while ΔE_{disp} is the contribution of the dispersion forces. ADF2014 has been used to decompose ΔE_{Pauli} and ΔE_{elst}, as requested from one of the referees (results are reported in the Supporting Information).

NBO analysis has been performed using the NBO6 suite of software.[60]

Charge Displacement function analysis. The Charge Displacement function analysis is based on Eq. (2).[25] $\Delta\rho(x,y,z)$ is the difference between the electron density of a complex and that of its non-interacting fragments placed in the same position as they occupy in the complex. In the present case, the fragmentation depends on the interaction under examination and are generally indicated in each case. The function $\Delta q(z')$ defines, at each point along a chosen axis, the amount of electron charge that, upon formation of the bond between the fragments, moves across a plane perpendicular to the axis through the point z'. A positive (negative) value corresponds to electrons flowing in the direction of decreasing (increasing) z. Charge accumulates where the slope of Δq is positive and decreases where it is negative.

$$\Delta q(z') = \int_{-\infty}^{+\infty} dx \int_{-\infty}^{+\infty} dy \int_{-\infty}^{z'} dz \Delta\rho(x,y,z) \quad (2)$$

where $\Delta\rho(x,y,z)$ is the difference between the electron densities of a complex and the sum of that of its non-interacting fragments, frozen at the same geometry they assume in the complex.

For C_{2v} symmetry-constrained systems, the chosen symmetry planes are that of the molecule and the plane perpendicular to the latter. This allows the separation of the net charge displacement $\Delta\rho$ into the contributing components, according to Eqs (3) and (4):

$$\Delta\rho = \sum_p \Delta\rho_p \tag{3}$$

$$\Delta\rho_p = \sum_{i\in p}\left|\phi_i^{(AB)}\right|^2 - \sum_{i\in p}\left|\phi_i^{(A)}\right|^2 - \sum_{i\in p}\left|\phi_i^{(B)}\right|^2 \tag{4}$$

where p labels the irreducible representations A_1, A_2, B_1 and B_2. AB, A and B represent the complex of the two fragments and the two separate fragments, respectively, while ϕ_i are the Kohn-Sham orbitals.
For non-symmetric systems, we make use of the natural orbital for chemical valence theory (NOCV):[29,48] $\Delta\rho$', which is different from the previously discussed $\Delta\rho$, is built from the occupied orbitals of A and B, suitably orthogonalized to each other and renormalized (*promolecule*), using the "valence operator" (Eq. 3),[61–63]

$$\hat{V} = \sum_i \left(|\psi_i^{(AB)}\rangle\langle\psi_i^{(AB)}| - |\psi_i^0\rangle\langle\psi_i^0|\right) \tag{3}$$

where ψ_i^0 is the set of the occupied Kohn−Sham orbitals of fragments A and B, mutually orthonormalized, and $\psi_i^{(AB)}$ is the set of occupied orbitals of the adduct. The NOCVs can be grouped in pairs of complementary orbitals (φ_k, φ_{-k}) corresponding to eigenvalues with same absolute value but opposite sign (Eq. 4).

$$\hat{V}\varphi_{\pm k} = \pm\nu_k\varphi_{\pm k}\ (\nu_k > 0) \tag{4}$$

where k numbers the NOCV pairs (k = 0 for the largest value of $|\nu_k|$). In this framework, $\Delta\rho$' can be defined as in Eq. 5.

$$\Delta\rho' = \sum_k \nu_k(|\varphi_k|^2 - |\varphi_{-k}|^2) = \sum_k \Delta\rho'_k \tag{5}$$

For each value of k, an energy contribution associated with the k-th NOCV pair is given. The most important ones are listed in the ESI.

Now the different $\Delta\rho'_k$ can be separately integrated using Eq. 2.[33]

The electronic density matrices have been mapped on a cube and manipulated through the suite of tools "Cubes".[64,65]

ACKNOWLEDGEMENTS

Università degli Studi di Pisa (PRA_2018_36 grant) is acknowledged for financial support.

REFERENCES

[1] G. R. Desiraju, P. S. Ho, L. Kloo, A. C. Legon, R. Marquardt, P. Metrangolo, P. Politzer, G. Resnati, K. Rissanen, *Pure Appl. Chem.* **2013**, *85*, 1711–1713.

[2] G. Cavallo, P. Metrangolo, R. Milani, T. Pilati, A. Priimagi, G. Resnati, G. Terraneo, *Chem. Rev.* **2016**, *116*, 2478–2601.

[3] P. Politzer, J. S. Murray, *ChemPhysChem* **2013**, *14*, 278–294.

[4] A. Mukherjee, S. Tothadi, G. R. Desiraju, *Acc. Chem. Res.* **2014**, *47*, 2514–2524.

[5] G. H.-Y. Lin, H. Hope, *Acta Crystallogr. Sect. B* **1972**, *28*, 643–646.

[6] R. Montis, M. Arca, M. C. Aragoni, A. Bauzá, F. Demartin, A. Frontera, F. Isaia, V. Lippolis, *CrystEngComm* **2017**, *19*, 4401–4412.

[7] H. S. El-Sheshtawy, M. M. Ibrahim, I. El-Mehasseb, M. El-Kemary, *Spectrochim. Acta - Part A Mol. Biomol. Spectrosc.* **2015**, *143*, 120–127.

[8] R. D. Parra, *Molecules* **2014**, *19*, 1069–1084.

[9] Y. Lu, J. Zou, H. Wang, Q. Yu, H. Zhang, Y. Jiang, *J. Phys. Chem. A* **2005**, *109*, 11956–11961.

[10] V. Vasylyeva, S. K. Nayak, G. Terraneo, G. Cavallo, P. Metrangolo, G. Resnati, **2014**, *16*, 8102–8105.

[11] F. Topić, K. Rissanen, *J. Am. Chem. Soc.* **2016**, *138*, 6610–6616.

[12] D. Cappelletti, E. Ronca, L. Belpassi, F. Tarantelli, F. Pirani, *Acc. Chem. Res.* **2012**, *45*, 1571–1580.

[13] F. Nunzi, D. Cesario, L. Belpassi, F. Tarantelli, L. F. Roncaratti, S. Falcinelli, D. Cappelletti, F. Pirani, *Phys. Chem. Chem. Phys.* **2019**, *21*, 7330–7340.

[14] D. Cappelletti, V. Aquilanti, A. Bartocci, F. Nunzi, F. Tarantelli, L. Belpassi, F. Pirani, *J. Phys. Chem. A* **2016**, *120*, 5197–5207.

[15] G. Ciancaleoni, F. Nunzi, L. Belpassi, *Molecules* **2020**, *25*, 300.

[16] G. Ciancaleoni, L. Biasiolo, G. Bistoni, A. Macchioni, F. Tarantelli, D. Zuccaccia, L. Belpassi, *Chem. - A Eur. J.* **2015**, *21*, 2467–2473.

[17] D. Marchione, M. A. Izquierdo, G. Bistoni, R. W. A. Havenith, A. Macchioni, D. Zuccaccia, F. Tarantelli, L. Belpassi, *Chem. - A Eur. J.* **2017**, *23*, 2722–2728.

[18] G. Bistoni, S. Rampino, N. Scafuri, G. Ciancaleoni, D. Zuccaccia, L. Belpassi, F. Tarantelli, *Chem. Sci.* **2016**, *7*, 1174–1184.

[19] L. Belpassi, I. Infante, F. Tarantelli, L. Visscher, *J. Am. Chem. Soc.* **2008**, *130*, 1048–1060.

[20] K. M. Azzopardi, G. Bistoni, G. Ciancaleoni, F. Tarantelli, D. Zuccaccia, L. Belpassi, *Dalt. Trans.* **2015**, *44*, 13999–14007.

[21] G. Ciancaleoni, L. Belpassi, F. Marchetti, *Inorg. Chem.* **2017**, *56*, 11266–11274.

[22] G. Ciancaleoni, C. Santi, M. Ragni, A. L. Braga, *Dalt. Trans.* **2015**, *44*, 20168–20175.

[23] W. Li, L. Spada, N. Tasinato, S. Rampino, L. Evangelisti, A. Gualandi, P. G. Cozzi, S. Melandri, V. Barone, C. Puzzarini, *Angew. Chemie Int. Ed.* **2018**, *57*, 13853–13857.

[24] F. Nunzi, D. Cesario, F. Pirani, L. Belpassi, G. Frenking, F. Grandinetti, F. Tarantelli, *J. Phys. Chem. Lett.* **2017**, *8*, 3334–3340.

[25] N. Salvi, L. Belpassi, F. Tarantelli, *Chem. - A Eur. J.* **2010**, *16*, 7231–7240.

[26] G. Bistoni, L. Belpassi, F. Tarantelli, *Angew. Chemie - Int. Ed.* **2013**, *52*, 11599–11602.

[27] M. J. S. Dewar, *Bull. Chem. Soc. Fr.* **1951**, *18*, C71–C79.

[28] J. Chatt, L. A. Duncanson, *J. Chem. Soc.* **1953**, *0*, 2939.

[29] M. Mitoraj, A. Michalak, *J. Mol. Model.* **2007**, *13*, 347–355.

[30] M. Radoń, *Theor. Chem. Acc.* **2008**, *120*, 337–339.

[31] M. Mitoraj, A. Michalak, *J. Mol. Model.* **2008**, *14*, 681–687.

[32] A. Michalak, M. Mitoraj, T. Ziegler, *J. Phys. Chem. A* **2008**, *112*, 1933–1939.

[33] G. Bistoni, S. Rampino, F. Tarantelli, L. Belpassi, *J. Chem. Phys.* **2015**, *142*, 084112.

[34] G. Marrazzini, C. Gabbiani, G. Ciancaleoni, *ACS Omega* **2019**, *4*, 1344–1353.

[35] G. Ciancaleoni, *ACS Omega* **2018**, *3*, 16292–16300.

[36] M. Mitoraj, A. Michalak, *Organometallics* **2007**, *26*, 6576–6580.

[37] M. Srebro, A. Michalak, *Inorg. Chem.* **2009**, *48*, 5361–5369.

[38] M. P. Mitoraj, A. Michalak, T. Ziegler, *J. Chem. Theory Comput.* **2009**, *5*, 962–975.

[39] F. Pirani, D. Cappelletti, S. Falcinelli, D. Cesario, F. Nunzi, L. Belpassi, F. Tarantelli, *Angew. Chemie - Int. Ed.* **2019**, *58*, 4195–4199.

[40] M. Novák, C. Foroutan-Nejad, R. Marek, *Phys. Chem. Chem. Phys.* **2015**, *17*, 6440–6450.

[41] P. L. Bora, M. Novák, J. Novotný, C. Foroutan-Nejad, R. Marek, *Chem. - A Eur. J.* **2017**, *23*, 7315–7323.

[42] M. P. Mitoraj, A. Michalak, *J. Mol. Model.* **2013**, *19*, 4681–4688.

[43] E. Buttarazzi, F. Rosi, G. Ciancaleoni, *Phys. Chem. Chem. Phys.* **2019**, *21*, 20478–20485.

[44] E. D. Glendening, C. R. Landis, F. Weinhold, *Wiley Interdiscip. Rev. Comput. Mol. Sci.* **2012**, *2*, 1–42.

[45] G. te Velde, F. M. Bickelhaupt, E. J. Baerends, C. Fonseca Guerra, S. J. A. van Gisbergen, J. G. Snijders, T. Ziegler, *J. Comput. Chem.* **2001**, *22*, 931–967.

[46] F. Neese, *Wiley Interdiscip. Rev. Comput. Mol. Sci.* **2017**, e1327.

[47] F. Neese, *Wiley Interdiscip. Rev. Comput. Mol. Sci.* **2012**, *2*, 73–78.

[48] A. Altun, F. Neese, G. Bistoni, *J. Chem. Theory Comput.* **2019**, *15*, 215–228.

[49] L. Carreras, J. Benet-Buchholz, A. Franconetti, A. Frontera, P. W. N. M. Van Leeuwen, A. Vidal-Ferran, *Chem. Commun.* **2019**, *55*, 2380–2383.

[50] D. W. Johnson, C. Carroll, M. M. Haley, J. Engle, *Tunable Phenylacetylene Hosts*, **2014**, US 20140031559 A1 20140130.

[51] M. Bedin, A. Karim, M. Reitti, A. C. C. Carlsson, F. Topić, M. Cetina, F. Pan, V. Havel, F. Al-Ameri, V. Sindelar, et al., *Chem. Sci.* **2015**, *6*, 3746–3756.

[52] G. Ciancaleoni, *Phys. Chem. Chem. Phys.* **2018**, *20*, 8506–8514.

[53] S. J. Grabowski, *Chem. Rev.* **2011**, *111*, 2597–2625.

[54] E. Aubert, E. Espinosa, I. Nicolas, O. Jeannin, M. Fourmigué, *Faraday Discuss.* **2017**, *203*, 389–406.

[55] M. L. Liriano, J. Carrasco, E. A. Lewis, C. J. Murphy, T. J. Lawton, M. D. Marcinkowski, A. J. Therrien, A. Michaelides, E. C. H. Sykes, *J. Chem. Phys.* **2016**, *144*, 094703.

[56] E. Van Lenthe, *J. Chem. Phys.* **1999**, *110*, 8943–8953.

[57] A. Bauzá, I. Alkorta, A. Frontera, J. Elguero, *J. Chem. Theory Comput.* **2013**, *9*, 5201–5210.

[58] S. Grimme, J. Antony, S. Ehrlich, H. Krieg, *J. Chem. Phys.* **2010**, *132*, 154104.

[59] M. von Hopffgarten, G. Frenking, *Wiley Interdiscip. Rev. Comput. Mol. Sci.* **2012**, *2*, 43–62.

[60] E. D. Glendening, J. K. Badenhoop, A. E. Reed, J. E. Carpenter, J. A. Bohmann, C. M. Morales, C. R. Landis, F. Weinhold, *NBO 6 (Theoretical Chemistry Institute, University of Winsconsin, Madison, WI, 2013); Http://Nbo6.Chem.Wisc.Edu/*, **n.d.**

[61] R. F. Nalewajski, A. M. Köster, K. Jug, *Theor. Chim. Acta* **1993**, *85*, 463–484.

[62] R. F. Nalewajski, J. Ozek, *Int. J. Quantum Chem.* **1994**, *51*, 187–200.

[63] R. F. Nalewajski, J. Mrozek, A. Michalak, *Int. J. Quantum Chem.* **1997**, *61*, 589–601.

[64] S. Rampino, *VIRT&L-COMM* **2015**, *7*, 6.

[65] A. Salvadori, M. Fusè, G. Mancini, S. Rampino, V. Barone, *J. Comput. Chem.* **2018**, *39*, 2607–2617.